

Mn²⁺/Mn³⁺ state of La_{0.7}Ce_{0.3}MnO₃ by oxygen reduction and photodoping

Andreas Thiessen, Elke Beyreuther,* Stefan Grafström, and Lukas M. Eng
Institut für Angewandte Photophysik, Technische Universität Dresden, D-01062 Dresden, Germany

Kathrin Dörr
*IFW Dresden, Institute for Metallic Materials,
Postfach 270116, D-01171 Dresden, Germany*
and

Institute for Physics, MLU Halle-Wittenberg, Von-Danckelmann-Platz 3, D-06120 Halle (S.), Germany

Robert Werner, Reinhold Kleiner, and Dieter Koelle
*Physikalisches Institut and Center for Collective Quantum Phenomena in LISA⁺,
Universität Tübingen, Auf der Morgenstelle 14, D-72076 Tübingen, Germany*
(Dated: December 9, 2013)

Films of cerium-doped LaMnO₃, which has been intensively discussed as an electron-doped counterpart to hole-doped mixed-valence lanthanum manganites during the past decade, were analyzed by x-ray photoemission spectroscopy with respect to their manganese valence under photoexcitation. The comparative analysis of the Mn 3s exchange splitting of La_{0.7}Ce_{0.3}MnO₃ (LCeMO) films in the dark and under illumination clearly shows that both oxygen reduction and illumination are able to decrease the Mn valence towards a mixed 2+/3+ state, independently of the film thickness and the degree of CeO₂ segregation. Charge injection from the photoconductive SrTiO₃ substrate into the Mn e_g band with carrier lifetimes in the range of tens of seconds and intrinsic generation of electron-hole pairs within the films are discussed as two possible sources of the Mn valence shift and the subsequent electron doping.

PACS numbers: 71.30.h, 72.40.w, 73.50.Pz, 75.47.Lx

I. INTRODUCTION

Mixed-valence manganites have been in the focus of extended research activities for decades due to their intriguingly manifold magnetic and electronic phases, high spin polarization, or the occurrence of the colossal magnetoresistance (CMR) effect in a number of such compounds¹⁻⁴. It is of fundamental academic interest to fully understand microscopically the strong coupling of different degrees of freedom, the resulting subtle phase equilibria, the sensitivity of the latter to external stimuli, as well as other peculiarities such as electronic phase separation or completely new physical properties in thin film heterostructures. Furthermore, some compounds, such as La_{0.7}Sr_{0.3}MnO₃ (LSMO), show high spin polarization at room temperature, which makes them interesting for applications in upcoming oxide-electronic devices.

In the past, most frequently hole-doped rare-earth manganites such as La_{1-x}Ca_xMnO₃ (LCMO), the above-mentioned La_{1-x}Sr_xMnO₃ (LSMO), Pr_{1-x}Ca_xMnO₃ (PCMO), or Pr_{1-x}Sr_xMnO₃ (PSMO) – all with 0 < x < 1, were investigated. There, in the parent compounds (LaMnO₃ or PrMnO₃, respectively) part of the trivalent rare earth ions (La³⁺ or Pr³⁺) are replaced by divalent cations such as Sr²⁺ or Ca²⁺. To preserve charge neutrality part of the originally trivalent Mn ions are forced into a tetravalent state, finally leading to a mixed Mn^{3+/4+} state, which corresponds to hole doping. The mixed Mn^{3+/4+} valence is crucial for the specific electronic transport mechanisms (e.g. the double-exchange

scenario) of the manganites and the strong coupling of magnetic order and electric transport.

With regard to possible all-oxide or even all-manganite devices, the question whether LaMnO₃ accepts a La³⁺ substitution by tetravalent cations such as Ce⁴⁺, Te⁴⁺, Sn⁴⁺ was raised around a decade ago. Nominally such a substitution would result in a mixed Mn^{2+/3+} state and electron doping. However, for the most intensively investigated case of Ce doping, it was found that single-phase materials can be grown only in the form of thin films in a limited range of doping concentrations⁵, because of the unfavorable ionic sizes of Ce⁴⁺ and Mn²⁺. While the most previous investigations deal with fundamental preparation^{6,7}, transport^{8,9}, magnetism⁹⁻¹¹, electronic structure¹²⁻¹⁵, or valence^{16,17} issues – always motivated by the question whether an electron-doping is really present or not – a few studies went a step further and focused on possible heterostructures including LCeMO films¹⁸⁻²⁰. A more detailed review of the debate was given in 21. In general, one can summarize, that La_{1-x}Ce_xMnO₃ (LCeMO) films tend to CeO₂ phase segregation and oxygen enrichment, the latter leading to an effective hole doping of as-grown films.

On the other hand, as discussed in our former XPS investigation²¹, oxygen reduction by heating in an ultrahigh-vacuum environment is a suitable way to drive the Mn valence towards 2+ /3+, which is, however, connected with a decisive resistance increase and the loss of an important functional property, namely the manganite-typical metal-insulator transition (MIT)²². As a fur-

TABLE I. Samples of this study: LCeMO-film parameters; the full details to sample A can be found in 21, the details concerning samples B, C, D in 26. Note, that transmission electron microscopy had shown nanoscopic cerium oxide clusters in B and C, which were not visible in the XRD results.

label	thickness (nm)	p(O ₂) (mbar)	XRD
A	10	0.53	single phase
B	30	0.25	single phase
C	100	0.25	single phase
D	100	0.03	CeO ₂ cluster

ther intriguing aspect, those oxygen-reduced, insulating, electron-doped LCeMO thin films exhibited a large photoconductivity and the recovery of the MIT, in contrast to the non-photosensitive as-grown hole-doped films.

Besides a number of microscopic explanations of intrinsic photoinduced effects in manganites (as summarized in 22 and 23), the injection of photogenerated charge carriers from the substrate^{22–25} seems to play a major and possibly technologically interesting role in thin-film-substrate heterostructures. In two studies of Katsu et al.^{24,25} La_{0.7}Sr_{0.3}MnO₃ films on SrTiO₃ were illuminated with a broad-band white-light source and exhibited a negative photoresistivity (PR), according to the definition $PR = (R_{dark} - R_{illum})/R_{illum}$.

The negative PR was interpreted as the injection of optically generated electrons from the SrTiO₃ substrate into the hole-doped film followed by the recombination of both carrier types in the film leading to a resistance increase. We picked up this stream of thinking in our two previous works, in which we observed a positive PR in La_{0.7}Ce_{0.3}MnO_{3- δ} ²² and La_{0.7}Ca_{0.3}MnO_{3- δ} ²³ films on SrTiO₃. By comparatively evaluating the wavelength dependence of the PR and the surface photovoltage we concluded that the photogenerated carriers must stem from interband transitions in the substrate or be excited from interface states.

In the present work, we aim at deepening our understanding of the light-induced charge carrier generation in a tetravalent-doped thin-film manganite. We performed a comparative investigation of the Mn valence of LCeMO films of different thicknesses on SrTiO₃ under broadband white-light illumination, by evaluating the Mn 3s exchange splitting in the x-ray photoemission spectrum in order to clarify the doping type under photoexcitation.

II. EXPERIMENTAL

A. Samples

Four different LCeMO films, in the following labelled A, B, C, D, and summarized in table I, were grown by pulsed laser deposition on SrTiO₃ (100) single crystal substrates. The substrates were 10×5×0.5 mm³ in size.

Sample A was already the subject of our previous investigations – the corresponding references^{21,22} contain the preparation details. The growth and structural analysis of samples B, C, D are given in 26. Samples B and C were grown under identical oxygen partial pressure of p(O₂)=0.25 mbar but are different in thickness, while samples C and D have the same thickness but D was grown under a much lower oxygen pressure, which led to microscopic segregation of CeO₂ clusters. Thus, the comparison of B and C provides information on the thickness dependence of the observed effects, while contrasting C and D is relevant to quantify the influence of the phase segregation.

To separate the influence of oxygen stoichiometry from any of the above parameters, each sample was studied in two different states of oxygen reduction, which were prepared by heating in a low-pressure oxygen atmosphere: A *slightly reduced* state was achieved by annealing the samples at 480 °C in 10⁻⁶ mbar oxygen partial pressure for 1 h, while a *highly reduced* state was prepared by heating at 700 °C in 10⁻⁸ mbar oxygen partial pressure for 2 h.

B. XPS measurements

The photoemission equipment for the XPS measurements uses a Mg anode and has been specified elsewhere²¹, where also details on the LCeMO overview spectra, surface cleaning, and background correction are elaborated. All spectra were recorded at room temperature.

For studying the effect of photoexcitation on the Mn core signals the respective sample was simultaneously illuminated by the broadband output of a Hg arc lamp providing a maximum intensity of 18.6 $\mu\text{W mm}^{-2}$ (integrated over the whole spectrum). Between 390 nm and 250 nm the integrated intensity measures 9.6 $\mu\text{W mm}^{-2}$. This interval is the spectral range relevant for band-to-band excitation of electrons in the SrTiO₃ substrate. The white light was focused by a fused-silica lens and transmitted through an UV-transparent viewport into the UHV apparatus.

In contrast to our former XPS work²¹, which was limited to one 10-nm-thick, gradually oxygen-reduced LCeMO film, now the Mn 3s exchange splitting energy ΔE_{3s} is measured for a whole set of LCeMO films, cf. table I, in two different states of oxygen reduction.

As pointed out earlier, the Mn valence V_{Mn} can be calculated from the measured value of ΔE_{3s} via the empirical equation:

$$V_{Mn} = 9.67 - 1.27(\text{eV})^{-1} \cdot \Delta E_{3s} \quad , \quad (1)$$

which is based on XPS results of a number of Mn compounds with well-known Mn valences^{27,28}.

As shown in figure 1(a), the intensity of the Mn 3s lines is comparably low and, more problematic, they are located in the direct neighborhood of the La 4d lines and

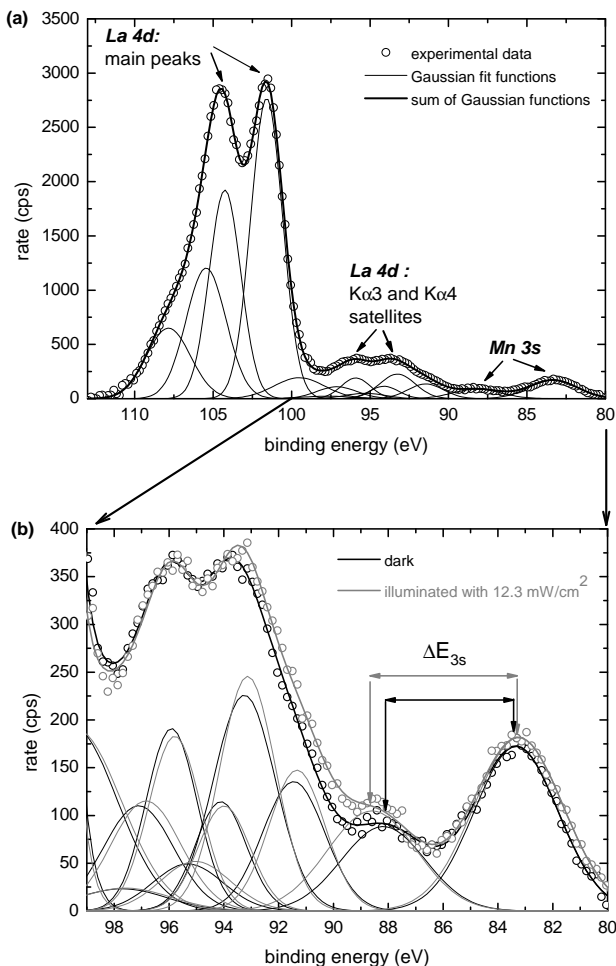


FIG. 1. (a) Mn 3s doublet and neighboring La 4d signals: Deconvolution into individual peaks in order to find a realistic value of the Mn 3s exchange splitting energy. (b) Increase of the Mn 3s exchange splitting energy under illumination in an oxygen-reduced LCeMO film.

part of their satellites. For large Mn 3s exchange splittings the smaller peak of the Mn 3s doublet even sits on the shoulder of the La 4d $K\alpha_3$ satellite. Consequently, the quantitative determination of ΔE_{3s} and thus V_{Mn} needs a careful deconvolution of the spectrum into the individual peaks of the La 4d and Mn 3s structures. The La 4d structure consists of four peaks and the corresponding $K\alpha_3$ and $K\alpha_4$ satellites. Together with the two peaks of the Mn 3s level this gives 14 peaks, each described by three parameters (position, height, and width). Thus, we obtain a regression function with 42 variables, which are fortunately not completely independent.

The La 4d signal is made up of four peaks with a fixed energetic separation and an intensity ratio between La $4d_{5/2}$ and La $4d_{3/2}$ of 0.69, which results in eight independent fit parameters, see²⁹. Since the $K\alpha_3$ and $K\alpha_4$ satellites are energetically shifted images of the original La 4d signal, they theoretically cannot have free parameters. However, due to the noise of the measured data,

it was necessary to treat the intensity and width of La $4d_{5/2}$ $K\alpha_3$ and the width of La $4d_{3/2}$ $K\alpha_3$ as free parameters initially – in order to make the regression algorithm more flexible. In practice, first the regression analysis³⁰ (based on the Levenberg-Marquardt algorithm) was performed for the whole La 4d structure, then the regression function was extended by the two Mn 3s peaks and the regression analysis was rerun. Figure 1(a) represents a typical result of the fitting procedure.

After the respective oxygen reduction procedure the sample was moved from the preparation chamber to the photoemission chamber – all in the same UHV apparatus – and an overview x-ray photoemission spectrum as well as a detailed spectrum of the region of a possible C 1s peak (as a test for possible organic contaminations) were taken. To study the influence of illumination on the Mn valence and to conclude on the nature of the photogenerated carriers, spectra of the La4d/Mn 3s region in the dark and afterwards under illumination were recorded. Figure 1(b) depicts two exemplary spectra of this region with and without light; the increase of the exchange splitting, which corresponds to a decrease of the Mn valence towards $2+/3+$ according to (1), is clearly visible.

Due to the weakness of the Mn 3s signal, noise influences the fitting results. Depending on the concrete case, each measurement was repeated between 5 and 13 times. For each of those measurements the sample was freshly prepared. Note that heating in oxygen-rich atmosphere approximately recovers the as-prepared state, as shown formerly²¹. In some selected cases, a second dark measurement was performed after the measurement under light excitation. There was no remarkable difference observed between the two dark values of the valence shift. Thus we can exclude that the valence shifts are caused by further outdiffusion of oxygen into the UHV surroundings. Finally, the mean values of V_{Mn}^{dark} , $V_{Mn}^{illuminated}$, and $\Delta V_{Mn} = V_{Mn}^{dark} - V_{Mn}^{illuminated}$ were statistically calculated based on 95% confidence intervals. Figure 2 and table II show the mean values and the confidential intervals (errors).

In the dark, as clearly visible in figure 2, the slight reduction procedure is not able to drive the Mn valence below +3, while the stronger reduction leads to Mn valences below +3 and thus indeed to an electron doping. This is in qualitative accordance with our previous study²¹. Within the error bars, it is hard to see systematic differences between the four individual samples. Besides the fact that the lowest Mn valence is achieved in the thinnest film, no serious systematic dependence on the thickness or the degree of phase segregation is visible.

Under illumination, both the slightly and the highly reduced films exhibit a *further* decrease of the Mn valence towards the mixed $2+/3+$ state, which is equivalent to a photoinduced increase of the electron density in the Mn- e_g orbital.

Importantly, control experiments with only-cleaned films in the dark and under illumination showed a mixed

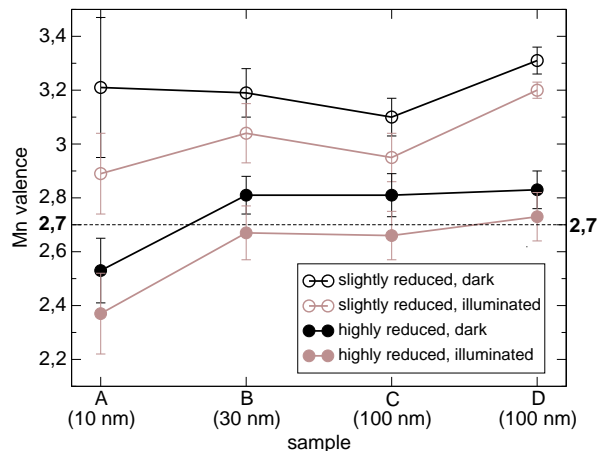


FIG. 2. Overview of the main results: Mn valence of the four LCeMO films in two states of oxygen reduction, in the dark and under illumination, respectively. For better orientation, the nominal value of 2.7 is depicted as dashed line.

TABLE II. XPS results of the light-induced Mn-valence shift ΔV_{Mn} , the amount of the corresponding injected charge carriers ΔN_{e_g} according to eq. (3) and the associated carrier lifetime τ . The latter are calculated using eq. (4) and assuming carrier injection from the substrate to be the dominant mechanism.

sample	reduction	ΔV_{Mn}	$\Delta N_{e_g} (\times 10^{15})$	τ (s)
A (10 nm)	slight	-0.32 ± 0.09	2.8 ± 0.8	2.9 ± 0.8
	high	-0.16 ± 0.08	1.4 ± 0.7	1.5 ± 0.7
B (30 nm)	slight	-0.15 ± 0.11	3.9 ± 2.9	4.1 ± 3.0
	high	-0.14 ± 0.04	3.6 ± 1.1	3.8 ± 1.2
C (100 nm)	slight	-0.15 ± 0.05	13.8 ± 4.2	13.8 ± 4.2
	high	-0.15 ± 0.08	13.8 ± 7.4	13.8 ± 7.4
D (100 nm)	slight	-0.11 ± 0.06	9.5 ± 5.3	9.5 ± 5.3
	high	-0.11 ± 0.03	9.5 ± 2.5	9.5 ± 2.5

3+/4+ valence and no change under illumination.

III. DISCUSSION

In general, at least two scenarios have to be discussed as possible explanations for the observed Mn valence decrease under illumination. First, the photoinduced generation of electron-hole pairs within the LCeMO films and a delayed recombination due to hole-trapping at oxygen vacancies, as already observed for other manganese compounds³¹, would be conceivable. Second, as pointed out earlier, for the 10-nm-thick LCeMO film, carrier injection from the substrate was suggested to be the main origin for the previously observed photoconductivity²². Here, all films show a similar shift of the Mn valence towards the electron-doped state under illumination. Thus it seems likely that the injection mechanism plays a role

also for the thicker films. Assuming a semiconductor band model, which has been successfully employed to explain a number of photoexcitation effects in manganites in the past, the samples are heterostructures of a wide-gap semiconductor (SrTiO_3 , $E_g=3.2$ eV) and a narrow-gap semiconductor (LCeMO, E_g around 1.0 eV), showing a band bending at the interface leading to a built-in field. Electron-hole pairs which are generated by photoexcitation in the substrate are separated by this field and the electrons can be injected into the LCeMO film.

In the following, the results for V_{Mn}^{dark} , $V_{Mn}^{illuminated}$, and ΔV_{Mn} are used to calculate the carrier densities n_{e_g} in the Mn- e_g orbitals of the LCeMO films according to:

$$n_{e_g} = \frac{3 - V_{Mn}}{a^3} \quad . \quad (2)$$

The lattice constant a measure 0.388 nm for samples A–C and 0.389 nm for sample D²⁶. The total number of charge carriers injected from the substrate into the film, ΔN_{e_g} , can be calculated as:

$$\Delta N_{e_g} = \frac{\Delta V_{Mn}}{a^3} \cdot V \quad , \quad (3)$$

with V being the volume of the film. The results for ΔN_{e_g} are listed in table II. Note that equations (2) and (3) are valid for the charge-injection as well as for the intrinsic-carrier-generation scenario.

Assuming ΔN_{e_g} to be the equilibrium number of photo-generated electrons in the film, the absorbed photon flux Φ and the life time τ are connected with ΔN_{e_g} via:

$$\Delta N_{e_g} = \Phi \cdot \tau \quad . \quad (4)$$

Using the charge-injection scenario, we can calculate τ from this relation. However, we have to be aware of the fact that the formula gives only a rough estimate of the carrier life times, since eq. (4) is only valid for a quantum efficiency for the electron-hole pair generation in the substrate of 100% and a simple exponential relaxation process. However, with the known flux of photons with energies above the SrTiO_3 bandgap of $\Phi = 9.45 \times 10^{14} \text{ s}^{-1}$ and under the assumption that all photons from the light source are absorbed in the SrTiO_3 bulk, life times between 1 and 10 s are calculated, see table II. Obviously, the life time increases with the film thickness. Within the mechanism postulated above this can be understood as follows: the spatial separation of the electron-hole pairs by the internal field prevents the electrons from recombining. For thicker films the mean distance of the electrons from the interface is larger and consequently the life time is longer. Similarly long life times (22 s) were also observed by Gao et al. in electron-doped $\text{La}_{0.8}\text{Te}_{0.2}\text{MnO}_3$ films on SrTiO_3 by analyzing the relaxation of the photoresistivity³². For the intrinsic-carrier-generation scenario, a serious value for Φ cannot

easily be determined, since the LCeMO absorption coefficients for the differently oxygen-reduced states are unknown. Thus, we are reluctant to estimate life times for this scenario.

Furthermore, we have to comment on why the illumination-induced Mn valence shift is exclusively seen in oxygen-reduced samples. In principle, this observation is compatible with both scenarios. For the intrinsic carrier generation scenario, the carrier (hole) trapping at oxygen vacancies is indeed essential. If there were no centers for pinning the holes, a fast recombination of the photogenerated electron-hole pairs could take place and would prevent the films from any electron doping – exactly as observed in the as-prepared case. However, the charge-injection scenario would be possible in the as-prepared (oxygen-rich) samples as well. At the current state of knowledge one may only speculate that the probably dramatically changed band alignment at the interface – note that SrTiO₃ changes from p-type in the ideal stoichiometric case to n-type under reduction – leads to very different recombination conditions.

Finally, possible systematic errors of the Mn valences due to the surface sensitivity of XPS measurements have to be considered. Taking into account that only the uppermost 2–3 nm of the films are probed and that former XAS results²⁶ revealed a higher Mn valence deeper inside the films than at their surfaces, the mean Mn valence can be higher than the values of table II. The finding that ΔV_{Mn} is independent of the film thickness might be, at least partially, an artifact produced by this systematic error.

IV. SUMMARY AND OUTLOOK

The Mn valence of 10-, 30-, and 100-nm-thick La_{0.7}Ce_{0.3}MnO₃ films was determined from the Mn 3s exchange splitting in the x-ray photoemission spectrum in the dark and under white-light illumination. Independ-

ent of the film thickness and the degree of CeO₂ segregation, both oxygen reduction and illumination turned out to be effective ways to drive the Mn valence towards 2+/3+ and thus make the LCeMO films electron-doped. Nevertheless, the two routes are not equivalent: While *oxygen reduction* alone drives the system towards a Mn valence below +3, *photoexcitation* lowers the Mn valence only in films with a certain *initial* degree of oxygen reduction.

Discussing (i) a scenario postulating charge injection from the photoconductive SrTiO₃ substrate into the Mn e_g band and (ii) a scenario assuming intrinsic photostimulated carrier generation and subsequent hole-trapping at oxygen vacancies within the LCeMO films as possible (and maybe coexisting) origins for the decreased Mn valence in LCeMO, we estimated the number of photo-generated injected carriers and their lifetimes in the films. To completely clarify which of the scenarios is the dominating one, a similar investigation of LCeMO on a non-photoconductive substrate as well as a more extended study of the spectral dependence of the photoconductivity than in ref. 22 would be illuminative.

The question whether electron-doped manganites can be established by tetravalent-ion doping can be answered as follows: It is not primarily the tetravalent doping ions but post-deposition oxygen reduction and – optionally – illumination which lead to an electron-doped state. The fact that reduction and illumination can induce an electron-doped state in divalent-ion-doped manganites (whose growth is commonly easier) as well²³ questions the need of tetravalent-ion substitution in manganites.

ACKNOWLEDGMENTS

This work was financially supported by the German Research Foundation (DFG, project no. BE 3804/2-1 and EN 434/31-1).

* elke.beyreuther@iapp.de

¹ A. Ramirez, J. Phys.: Condens. Matter **9**, 8171 (1997).

² J. M. D. Coey, M. Viret, and S. von Molnár, Adv. Phys. **48**, 167 (1999).

³ A.-M. Haghiri-Gosnet and J.-P. Renard, J. Phys. D: Appl. Phys. **36**, R127 (2003).

⁴ K. Dörr, J. Phys. D: Appl. Phys. **39**, R125 (2006).

⁵ P. Raychaudhuri, C. Mitra, P. D. A. Mann, and S. Wirth, J. Appl. Phys. **93**, 8328 (2003).

⁶ C. Mitra, P. Raychaudhuri, J. John, S. K. Dhar, A. K. Nigam, and R. Pinto, J. Appl. Phys. **89**, 524 (2001).

⁷ T. Yanagida, T. Kanki, B. Vilquin, H. Tanaka, and T. Kawai, Phys. Rev. B **70**, 184437 (2004).

⁸ P. Mandal and S. Das, Phys. Rev. B **56**, 15073 (1997).

⁹ P. Raychaudhuri, S. Mukherjee, A. K. Nigam, J. John, U. D. Vaisnav, R. Pinto, and P. Mandal, J. Appl. Phys. **86**, 5718 (1999).

¹⁰ J. R. Gebhardt, S. Roy, and N. Ali, J. Appl. Phys. **85**, 5390 (1999).

¹¹ B. W. Lee, K. Y. Seo, Y. J. Kim, H. Han, H. H. Lee, J. C. Han, S. Y. Park, and C. S. Kim, J. Magn. Magn. Mat. **226-230**, 803 (2001).

¹² B. I. Min, S. K. Kwon, B. W. Lee, and J.-S. Kang, J. Electron Spectrosc. Rel. Phenom. **114-116**, 801 (2001).

¹³ V. L. Joseph Joly, P. A. Joy, and S. K. Date, J. Magn. Magn. Mat. **247**, 316 (2002).

¹⁴ C. Mitra, Z. Hu, P. Raychaudhuri, S. Wirth, S. I. Csiszar, H. H. Hsieh, H.-J. Lin, C. T. Chen, and L. H. Tjeng, Phys. Rev. B **67**, 092404 (2003).

¹⁵ S. W. Han, J. D. Lee, K. H. Kim, C. Mitra, J. I. Jeong, K. J. Kim, B. I. Min, J. H. Kim, S. C. Wi, and J.-S. Kang, Phys. Rev. B **69**, 104406 (2004).

¹⁶ J. Philip and T. R. N. Kutty, J. Phys.: Condens. Matter **11**, 8537 (1999).

- ¹⁷ J.-S. Kang, Y. J. Kim, C. G. Olson, and B. I. Min, *J. Phys.: Condens. Matter* **13**, 3779 (2001).
- ¹⁸ C. Mitra, P. Raychaudhuri, G. Köbernik, K. Dörr, K.-H. Müller, L. Schultz, and R. Pinto, *Appl. Phys. Lett.* **79**, 2408 (2001).
- ¹⁹ C. Mitra, P. Raychaudhuri, K. Dörr, K.-H. Müller, L. Schultz, P. M. Oppeneer, and S. Wirth, *Phys. Rev. Lett.* **90**, 017202 (2003).
- ²⁰ H. Chou, Z. Y. Hong, S. J. Sun, J. Y. Juang, and W. J. Chang, *J. Appl. Phys.* **97**, 10A308 (2005).
- ²¹ E. Beyreuther, S. Grafström, L. M. Eng, C. Thiele, and K. Dörr, *Phys. Rev. B* **73**, 155425 (2006).
- ²² E. Beyreuther, A. Thiessen, S. Grafström, L. M. Eng, M. C. Dekker, and K. Dörr, *Phys. Rev. B* **80**, 075106 (2009).
- ²³ E. Beyreuther, A. Thiessen, S. Grafström, K. Dörr, and L. M. Eng, *J. Phys.: Condens. Matter* **22**, 175506 (2010).
- ²⁴ H. Katsu, H. Tanaka, and T. Kawai, *Appl. Phys. Lett.* **76**, 3245 (2000).
- ²⁵ H. Katsu, H. Tanaka, and T. Kawai, *J. Appl. Phys.* **90**, 4578 (2001).
- ²⁶ R. Werner, C. Raisch, V. Leca, V. Ion, S. Bals, G. Van Tendeloo, T. Chassé, R. Kleiner, and D. Koelle, *Phys. Rev. B* **79**, 054416 (2009).
- ²⁷ L. Z. Zhao and V. Young, *J. Electron Spectrosc. Relat. Phenom.* **34**, 45 (1984).
- ²⁸ V. R. Galakhov, M. Demeter, S. Bartkowski, M. Neumann, N. A. Ovechkina, E. Z. Kurmaev, N. I. Lobachevskaya, Y. M. Mukovskii, J. Mitchell, and D. Ederer, *Phys. Rev. B* **65**, 113102 (2002).
- ²⁹ W.-Y. Howng and R. J. Thorn, *Chem. Phys. Lett.* **56**, 463 (1978).
- ³⁰ “fityk,” Open-source software, available at <http://fityk.nieto.pl>.
- ³¹ A. Gilabert, R. Cauro, M. G. Medici, J. C. Grenet, H. S. Wang, Y. F. Hu, and Q. Li, *J. Supercond.* **13**, 285 (2000).
- ³² G. Gao, C. Chen, L. Han, and X. Cao, *J. Appl. Phys.* **105**, 033707 (2009).